Gas transport and characterization of poly(3 hydroxybutyrate) films

Article *in* European Polymer Journal · April 2017

DOI: 10.1016/j.eurpolymj.2017.03.047

5 authors, including:

Carlo Ingrao

Kore University of Enna

40 PUBLICATIONS **180** CITATIONS

SEE PROFILE

European Polymer Journal 91 (2017) 149–161

Contents lists available at ScienceDirect

European Polymer Journal

journal homepage: www.elsevier.com/locate/europolj

Gas transport and characterization of poly(3 hydroxybutyrate) films

Valentina Siracusa[a,*], Carlo Ingrao[a], Svetlana G. Karpova[b], Anatoly A. Olkhov[c,d], Alexey L. Iordanskii[c]

[a] Department of Chemical Science, University of Catania, Viale A. Doria 6, 95125 Catania (CT), Italy
[b] Emanuel Institute of Biochemical Physics, Kosygin Str. 4, Moscow 119991, Russian Federation
[c] Semenov Institute of Chemical Physics, Kosygin Str. 4, Moscow 119991, Russian Federation
[d] Plekhanov Russian University of Economics, Stremyanny per. 36, Moscow 117997, Russian Federation

ARTICLE INFO

Keywords:
Poly(3-hydroxybutyrate) (PHB)
Polyesters
Biomaterials
Structure-property relations
Barrier
Gas permeation

ABSTRACT

Renewable biodegradable films of poly(3-hydroxybutyrate) (PHB) were produced via thermo-compression and casting method (specimens 1 and 2). On specimens 1, gas permeability coefficients with CO_2, O_2, N_2, and C_2H_4 gases were measured at 277 K, 288 K and 296 K. The physicochemical characteristics of PHB based on calorimetric, mechanical, and thermal examination were performed for both specimens. SEM and probe ESR technique showed the dramatic differences in their surface morphology and segmental motilities in polymer bulk. In the selected temperature range, the gas permeability ranking (P_i) for the thermo-compressed films is as follows: $P(CO_2) > P(O_2) > P(N_2) \approx P(C_2H_4)$. The gas diffusion coefficients were considered to be dependent on the gas critical volume, in accordance with the semi-logarithmic function, consistent with a free volume model. The activation energies of permeability, diffusivity and spin probe rotation, as well as the apparent heat of sorption equilibrium, forecast the values of PHB barrier characteristics in the range of foodstuffs stored temperatures.

1. Introduction

Currently, petrochemical polymers engage an essential segment in the area of barrier materials, especially as packaging materials [1]. Owing to the availability of resources, a low market cost, appropriate mechanical behaviour, and gas selectivity, they have been widely used as special materials in biomedicine, membrane separation, and packaging industry [2–4]. In spite of those advantages, petrochemical polymers used as packages, coating films, and containers cause a few intrinsic challenges. Among the latter, there are two principal tasks: (i) their industrial manufacturing is based upon non-renewable fossil resources, which have been progressively depleting, and (ii) after the lifetime and successive land filling, they are accumulated as non biodegradable wastes. These and other inconveniences bring about the search for eco-friendly packaging formulations, based on biodegradable polymers [5–8]. Biopolyesters, such as poly(α-hydroxyacides), namely polylactides (PLA), and poly(β-hydroxyacides), namely polyhydroxybutyrate (PHB) as the main homolog of the family, offer attractive alternatives as long as their characteristics can be tailored to packaging application.

Both families of the biopolyesters have been comprehensively explored along the years as thermoplastic and biodegradable systems with relevant mechanic characteristics and biocompatibility. The principal claims of PHB are that it is obtained from

* Corresponding author.
E-mail address: vsiracus@dmfci.unict.it (V. Siracusa).

http://dx.doi.org/10.1016/j.eurpolymj.2017.03.047
Received 23 August 2016; Received in revised form 8 March 2017; Accepted 23 March 2017
Available online 02 April 2017
0014-3057/

renewable resources and can be enzymatically degraded in many ecosystems, such as soil, sewage sludge and sea water [9]. Because of high crystallinity and low gas permeability as well as owing to biocompatibility, PHB was intensively explored as promising barrier packaging material in biomedicine and food industry [10–14].

Along with the positive features of PHB, there are some inconveniences related to its fragility, low ductility and relatively high cost. Optimization of mechanical characteristics is related with the control of crystallinity degree, which depends upon the thermo-mechanical history and the way of polymer processing (casting, molding, rolling, etc.). Besides the mechanical behaviour, for PHB as barrier material there is another important aspect related to gas transport characteristics, which determine direct its application in different packaging sectors, especially in food packaging area.

To date, a limited number of publications have been developed to assess the issue of transport in PHB and its copolymers, and most of those describe water diffusion in biopolymers [15–17]. This situation is quite clear because, being PHB biodegradable, it is structurally sensitive to water molecules on chemical (bond cleavage) and morphological (physical age) levels. Conversely, experimental data on PHB permeability and diffusion of organic vapours and especially transport of gases are extremely poor. The exception is a few recent papers and comprehensive series of communications where the gas barrier characteristics of PHB are represented as auxiliary information for development of PLA-PHB blend packaging [18–24]. A somewhat large numbers of works on gas transport are devoted to the study of PLA, a polyester with structure and kinetic behaviour similar to PHB [22,23,25–27]. However, the use of the permeability PLA results for predicting the gas barrier features in PHB would not be quite correct, since in spite of the similarity of their molecular structures, there are real differences in the glass transition temperatures, crystallinity degree, and molecular stereo-regularity.

Thus, the study discussed in this paper was aimed at performing an in-depth analysis of the transport characteristics of PHB and foremost its permeability to several atmospheric gases. The presented results assess the PHB application as potential material for food packaging or biomedicine field. Besides, kinetic investigations will be accompanied by structural and physical chemical characteristics, combined with probe Electron Spin Resonance (ESR) spectroscopy technique to estimate segmental dynamic of PHB molecules [28].

2. Material and methods

2.1. Materials

The PHB was kindly presented by Biomer Co (Krailing, Germany), as lot 16F. The initial polymer was in the form of white powder with particle size of 5–7 μm, MW = $2.06 \cdot 10^5$ Da. Samples of PHB were prepared following the two procedures discussed below. In particular, PHB films (specimens 1) were prepared by thermo-compression molding using a manual hydraulic press with heated platens, manual thermostat control and maximum pressure of 25 MPa. First, the press was pre-heated at 150 °C and then the PHB powder was placed in a stainless steel frame with top and bottom covers (50 × 50 × 1.0 mm). Films were obtained at 12 MPa of pressure during 3 min at 172 °C. To prevent the molded film adhesion to the metal surface and promote sample detaching, the polyimide film (Kapton DuPont) was used.

Specimen 2 was dissolved in chloroform (5% wt/v) under stirring at 70 °C. Then it was cast from chloroform solution (5 wt.% PHB) on glass plate under slow evaporation (for 24 h) at room temperature. The obtained films were dried in vacuum to constant weight and then stored at least 2 weeks at room temperature.

The stable nitroxide radical, 2,2,6,6-tetramethyl-1-piperidinyloxyl (TEMPO), was absorbed from the gas phase in the special glass set. The concentration of the TEMPO in PHB was $3.7 \cdot 10^{17}$ spin cm^{-3} (PHB).

For greater rank of detail, Fig. 1 was reported to show the chemical formula of both the PHB and TEMPO.

2.2. Polymer preparations

Samples of PHB were prepared following the two procedures presented below. In particular, PHB films (specimens 1) were prepared by thermo-compression molding using a manual hydraulic press with heated platens, manual thermostat control and maximum pressure of 25 MPa. First, the press was pre-heated at 150 °C and then the PHB powder was placed in a stainless steel frame

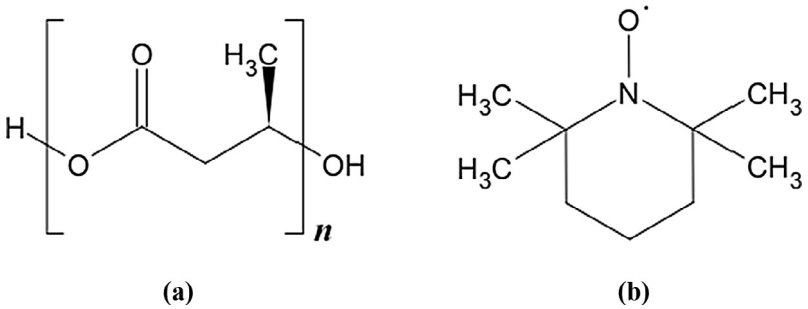

Fig. 1. Chemical formula of both PHB (a) and 2,2,6,6-tetramethyl-1-piperidinyloxyl (b) (TEMPO).

with top and bottom covers (50 × 50 × 1.0 mm). Films were obtained at 12 MPa of pressure during 3 min at 172 °C. To prevent the molded film adhesion to the metal surface and promote sample detaching, the polyimide film (Kapton DuPont) was used.

Specimen 2 was dissolved in chloroform (5% wt/v) under stirring at 70 °C. Then it was cast from chloroform solution (5 wt.% PHB) on glass plate under slow evaporation (for 24 h) at room temperature. The obtained films were dried in vacuum to constant weight and then stored at least 2 weeks at room temperature.

2.3. Thickness determination

The film thickness was determined using the Sample Thickness Tester MarCator 1086 (Mahr GmbH Esslingen), consisting of a digital indicator connected to a PC. The reading was made twice per second (the tool automatically performs at least three readings), measuring a minimum, a maximum and an average value with a resolution of 0.001 μm. The reported results represent the mean value thickness of three experimental tests run at 10 different points on the film surface, at room temperature.

2.4. Scanning electron microscopy

The morphological features of the two PHB specimens, obtained from the melt or by solution casting, were revealed by scanning electron microscopy (SEM). The electron micrographs were obtained on a JSM-5300LV electron microscope (JEOL). Film samples were contrasted by deposition of gold in a plasma discharge in a GSC-1100E system.

2.5. Colour characterization

The colour of film samples was measured using a HunterLab ColorFlex EZ 45/0° colour spectrophotometer, with D65 illuminant, 10° observer (according to ASTM E308). Measurements were made using CIE Lab scale. The instrument was calibrated with a black and white tile before the measurements. Results were expressed as L^* (lightness), a^* (red/green) and b^* (yellow/blue) parameters. The total colour difference (ΔE) was calculated as:

$$\Delta E = \sqrt{[(\Delta L^*)^2 + (\Delta a^*)^2 + (\Delta b^*)^2]}$$

where ΔL^*, Δa^* and Δb^* are the differentials between a sample colour parameter and the colour parameter of a standard white plate used as the film background. In particular:

$L^* = 92.62 \pm 0.01$, $a^* = 1.33 \pm 0.02$, and $b^* = 1.35 \pm 0.07$.

In addition, the chromaticity is labeled as C^* and is calculated as $\sqrt{[(a^*)^2 + (b^*)^2]}$, and the hue angle h_{ab} is calculated as $\tan^{-1}(a^*/b^*)$, according to Galus and Lenart [29] and Syahidad et al. [30]. Measurements were carried out in triplicate at random positions over the film surface and average values were calculated.

2.6. Differential scanning calorimetry (DSC) measurements

Thermophysical data (the enthalpies and the temperatures of thermoinduced transitions) were determined by DSC method with the Pyris DSC-6 calorimeter (Perkin-Elmer, USA) equipped with a liquid sub ambient accessory and calibrated with high purity standards, such as Indium and Tin. Polymer films were cut into small pieces of 2 mm^2 (5–10 mg) and then placed in a 50 μL sealed aluminum crucibles. In order to avoid film contamination, the special care was taken during specimen handling, namely working with gloves and manipulating with tweezers. After isothermal storing for 3 min at −20 °C, the weighed samples were heated with a scanning rate of 10 °C min^{-1} from −20 to 180 °C (*first scan*) and then, after a further isotherm of 3 min at 180 °C, were quenched to −20 °C at a rate of 100 °C min^{-1}. Finally, after an isotherm conditioning at this temperature for 5 min, samples were reheated from −20 °C to the same temperature as the first scan, at a heating rate of 10 °C min^{-1} (*second scan*). All experiments were performed under nitrogen flow (20 cm^3 min^{-1}). The melting temperature (T_m) and the crystallization temperature (T_c) were determined as the peak values on the DSC curves. The melting enthalpy (ΔH_m) of the crystal phase was calculated based on the area of the DSC endothermic peak as well as the crystallization enthalpy (ΔH_c). T_m and T_c values are well reproducible as result of the second scan, while those relating to the first scan are affected by thermal and mechanical history to which the samples were subjected. T_g and Δ_{cp} data were obtained from the second scan. Calorimetric analysis was performed on films samples triply.

The degree of crystallinity (x_C) was determined by using Eq. (1) as reported below

$$x_C = 100 \times \frac{\Delta H_m - \Delta H_C}{\Delta H_m^c} \quad (1)$$

where ΔH_m is the enthalpy of fusion and ΔH_c is the enthalpy of crystallization, ΔH_m^c is the heat of melting of purely crystalline PHB considering this value as 146 J g^{-1} [31].

2.7. Mechanical characterization

Tensile testing of the copolymers was performed using a Zwick Roell Texture machine, equipped with a rubber grip and controlled by a computer. A pre-load of 1 MPa was used with a pre-load speed of 5 mm/min. A 500 N load cell was used. Stress-strain tests

measurements were performed on rectangular films, of 5 mm wide and 50 mm high, with an initial grip-to-grip separation of 23 mm. The tensile stress-strain measurements were performed with a crosshead speed of 50 mm/min. Six different samples from the same film were tested for each copolymer composition and the results were provided as the average value ± standard deviation. All tests were carried out in accordance with ASTM D638 for film thickness below 100 μm.

2.8. ESR characterization

The quartz tubes with inner diameter 0.3 cm were filled by solid PHB films loaded with TEMPO from gas-phase at 40 °C and then flame sealed by the gas-jet. ESR spectra were recorded with Radiopan SE/X-2544 spectrometer (X-band) operating under the high-frequency modulation (100 kHz), on line with an IBM ICP-made system for data processing. The spectrometer was equipped with a home-made gas (N_2) flow thermostat. The spectra was received at selected temperatures within the range 296–358 K of the microwave power in resonator < 7 mW in order to avoid the saturation effect. The maximal modulation amplitude did not exceed 0.5 G that is essentially less than the minimum width of any resonance curves. The ESR spectra of TEMPO treated as averaged probe rotation ones give possibility to estimate rotational correlation times (τ_c) in various polymer specimens using the relationship [32,33]:

$$\tau_c = \Delta H_+ \times [\sqrt{(I_+/I_-)} - 1] \times 6.65 \times 10^{-10} \quad (2)$$

In Eq. (2), τ_c is espresse as [s/rad]; and ΔH_+ is the line width of the low-field component for X-band ESR spectra (in G) and I_+/I_- is the amplitude ratio of the low-field and high-field respectively. The error of τ_c measurement is ± 5%.

Beyond the range of fast rotation ($5 \cdot 10^{-11} < \tau_c < 10^{-9}$), the modeling of experimental ESR spectra was performed in the framework of the isotropic Brownian rotation approach proposed in with corresponding principal tensor and STS constants: g_{xx} = 2.0096, g_{yy} = 2.0066, g_{zz} = 2.0025, A_{xx} = 7.0 G, A_{yy} = 5.0 G, A_{zz} = 35.0 G [33,34].

2.9. Barrier properties evaluation

Permeability was measured by a manometric method using the Permeance Testing Device, type GDP-C (Brugger Feinmechanik GmbH, Germany), according to ASTM 1434-82 (Standard test Method for Determining Gas Permeability Characteristics of Plastic Film and Sheeting), DIN 53 536 in compliance with ISO/DIS 15 105-1 and following Gas Permeability Testing Manual (Registergericht München HRB 77,020, Brugger Feinmechanik GmbH, Germany). For permeability measuring, the film sample was placed between two vertically-mounted chambers. The upper upstream chamber was filled with the pure gas used in the test (CO_2, O_2, N_2 and C_2H_4), at pressure 1 atm. A pressure transducer, set in the downstream chamber, recorded the increase of gas pressure as a function of time. From the pressure-time plot, the software automatically monitors the gas flux, which has been converted in permeability meanings. The gas transmission rate (GTR) was expressed in $cm^3\,m^{-2}\,day^{-1}\,bar^{-1}$. Besides the permeability data, the time lag (t_L), which is required for the determination of diffusion coefficient (D) and solubility (S) of the tested gases were measured according to the mathematical relations reported in literature [35,36].

The sample temperature was set by an external thermostat, HAAKE-Circulator DC10-K15 type. Fluctuation of temperature values during the test was controlled by special hardware and software for an automatic temperature compensation that minimizes GTR deviations. All measurements were carried out at 23 °C (room temperature), 4 °C (simulating condition of fresh cut vegetable food storage temperature) and 15 °C (abusing temperature) [37,38].

The operative conditions were as follows: gas stream of 100 $cm^3\,min^{-1}$; 0% RH in any penetrating gas; sample area of 0.785 cm^2. All permeability measurements were performed triply at least and the mean value was submitted.

3. Results and discussion

3.1. PHB characterization by scanning electron microscopy

Scanning electron microscopy (SEM) is one of the principal techniques for polymer characterization owing to its ability to provide morphology of barrier film surfaces at submicron resolution. The resolution of SEM can reveal the fine details of PHB morphology coherently related to both transport and mechanical properties of the packaging material. To gain insight into the morphology of PHB films prepared by two different methods, SEM technique was used to obtain micrographs of the biopolymer surfaces. The structure of PHB films is built up of two kinds of clearly represented globules, as reported in Fig. 2a and b, respectively. The surface polymer pattern of the cast films consists of adjoining and slightly deformed globules. Their diameters vary from several micrometers to ~20 μm. Because of the incoherent arrangement of micro-particles forming the PHB matrix, the amount of pores results as relatively high though their lengths are limited: such is attributed to all pores being one-side open systems. All particles are characterized by the fine surface structure as conglomerates of tiny elements, which could be clearly distinguishable. The diameters of these elements correspond to the submicron range and are close to the diameters of natural PHB globules formed within the bacterial producers [39,40].

The opposite situation was observed for PHB films molded near the melting temperature. As a result of applying this method, the surfaces of PHB films acquired a uniform pattern with single or coalescing spherical particles. The boundary between the continuous phase and globules is clearly seen, however, all spherical particles are tightly incorporated into the basic polymer matrix. In some

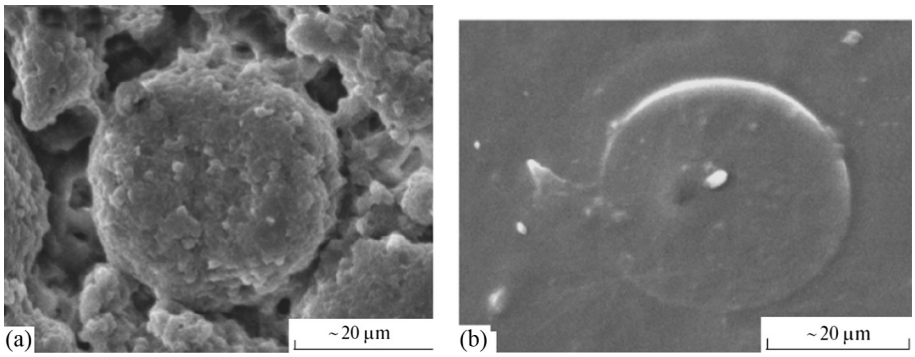

Fig. 2. Surface SEM micrographs of PHB films prepared from solution via slow evaporation of chloroform (a) and molding at 172 °C (b).

cases, the coalescence of the globules is absent and morphological elements are not in contact with each other, as can be seen from Fig. 2b. All of these structures are characterized by a spherical geometry of particles, which can create additional resistance to the gas permeation. In contrast to cast films, the effect of porosity is absent and the gas permeability should be predominantly controlled by diffusivity and thermodynamic solubility of penetrant.

3.2. Colorimetric properties of PHB films

Sensory aspects are essential to ensure that emerging technologies of PHB as packaging material become successful. The colour as an intrinsic characteristic of packaging material is one of the most important parameters to be carefully controlled. During food packaging, films should be as close to colourless state as possible, because calorimetric aspect influences on consumer acceptability immediately. PHB films are clear but they have different transparency. In order to evaluate the difference in colorimetric behaviour, lightness (L^*), colour values (a^* and b^*), chromaticity (C^*) and hue angle (h_{ab}) of the two PHB samples were determined. The obtained results were reported in the Table 1.

Specimen 2 shows an L^* value more related to white colour in respect to specimen 1, due to its higher crystallinity (lower ΔE value). From a^* and b^* values could be noted that the films showed a slight yellowish tendency (h_{ab} values over 90°) and a low C^* value, meaning that with a low colour saturation the films display a light yellow hue.

While the specimen 1 is almost clear (a^* near zero) and not totally transparent (high L^* value), with a higher tendency to yellowness (higher b^* value), the specimen 2 shows increase in L^* (decreasing of translucency) approaching to a white colour, clear (a^* near zero) and with a lower tendency to yellowness (lower b^* value). High lightness was observed for the specimen 2. The difference in the total colour, ΔE, indicates that specimen 2 has a tendency to the whitening, approaching ΔE value to zero. Chromaticity is the important quality of the colour, as it determines both saturation and intensity of the colour itself. In this regard, it was found that the colour saturation is very low for both films but higher for the film with a higher transparency where the chromatic part is more consistent than the achromatic ones. A decrease in chromaticity is related to a decrement of translucency. The hue angle is the main property that describes a dimension of the colour for the film samples. It is coherently associated with a^* and b^* values which are the physical characteristics used to indicate the visual colour.

From the data recorded, it should be concluded that the operative procedure via melting or casting gives rise to a different films appearance, with subsequent different crystallinity percentage, which is the main physical parameter influencing the colour behaviour. Arrieta [23] reported the calorimetric parameters for a commercial PHB used to prepare ternary PHA-PHB-limonene blends. Neat PHB sample showed an amber colour with slight transparency. The small but positive value in a^* (1.49 ± 0.87) showed a slight trend to red while positive value of b^* (22.48 ± 3.34) indicated a higher trend to yellow.

3.3. Thermal characterization of PHB specimens

High-temperature fragments of DSC curves for specimens 1 and 2 were depicted in Fig. 3a and b respectively. Two consecutive scans were carried out to determine the endothermic features, namely the melting temperature (T_m), and the crystallinity degree (x_c), for each of the analyzed films. The first scan gives information on thermal history of the specimens, while the second scan could delete the previous morphological feature as the consequence of thermal history and shows the polymer ability to re-crystallize after the first scan condition. The corresponding characteristics were shown in Table 2.

Table 1
L^*, a^*, b^*, total colour difference (ΔE), C^* and h_{ab} for 1 and 2 PHB specimen.

Film	L^*	a^*	b^*	ΔE	C^*	h_{ab}
Specimen 1	89.61 ± 0.21	−1.68 ± 0.02	4.46 ± 0.24	4.34	4.77	110.64
Specimen 2	93.97 ± 0.04	−0.89 ± 0.02	3.02 ± 0.03	2.20	3.15	106.42

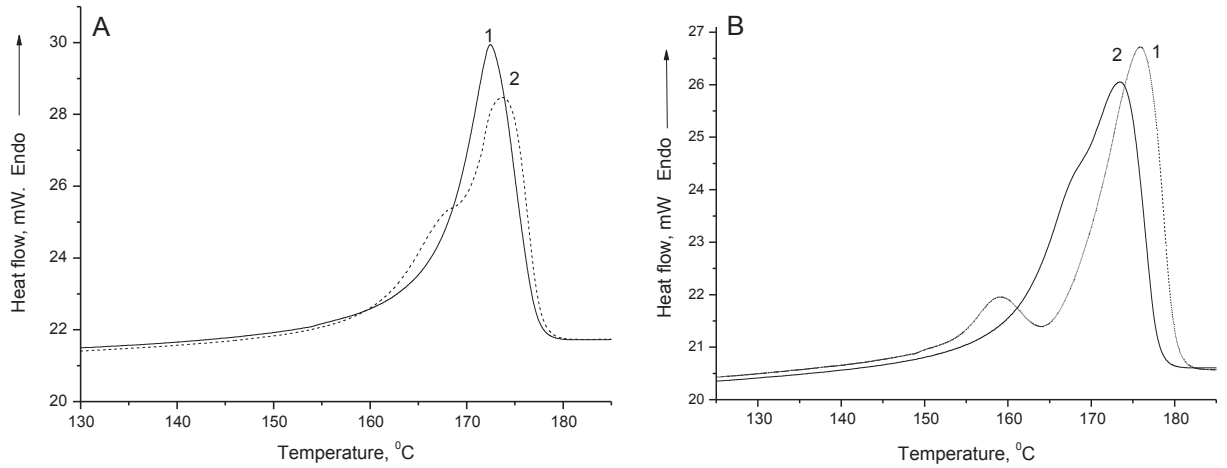

Fig. 3. (a) and (b) DSC curves for two PHB specimens 1(a) and 2(b). The two scans are presented.

For specimen 2 the DSC thermogram of the first scan shows two endothermic peaks, which are most probably related to the fusion of more perfect crystals (176 °C) and less perfect crystals (158 °C) respectively, according to Righettia and Di Lorenzo [41]. During the first scan, the high-temperature peak appears as a result of primary crystallization, while the low temperature peak reflects the secondary PHB crystallization [42–44]. This crystalline population developed probably during crystallization from the polymer solution, at ambient temperature. The specimen 1, prepared via thermo-pressing, resulted as characterized by a single melting peak, showing a more homogeneous structure of the crystalline phase. This morphology is very stable and so, after first scan, the polymer crystallinity and the melting point position do not change. Both DSC curves, the first and the second scan, are practically coincident each other. Owing to relatively high crystallinity, the PHB specimens do not exhibit the distinct transition related to glassy state temperature.

As it can be observed from the combination of SEM and DSC data, specimen 2 presents a poor structural order confirmed by the presence of two melting peak on the DSC curve associated with perfect and imperfect crystalline organizations and globular morphology, as also demonstrated on the micrograph in Fig. 2.

3.4. Mechanical characterization of PHB

The films intended for packaging applications undergoes a stressed treatment during packaging procedure and following exploitation; therefore, it is important to obtain principal mechanical characteristics of PHB films such as their elastic modulus (E), tensile stress (σ) and tensile strain (ε). Moreover, stressed films require optimal elasticity to avoid perforation during transportation and lifecycle use. To receive the mechanical features of the PHB films, the appropriate tests were performed (refer to Table 3). For the PHB samples tested, the Young modulus resulted to be significantly higher than that for the PLA and even higher than for PHB samples described in literature [22]. Elongation was quite low, showing a high rigidity of the samples, confirmed by the DSC results, due to a high degree of crystallinity. These results corroborate that the film obtained after thermal treatment at 172 °C shows a higher rigidity and strain, owing to its more perfect physical structure.

3.5. ESR characterization of PHB specimens

To ascertain the impact of PHB medium upon the magnetic behaviour of the nitroxyl radical probe (TEMPO), the ESR spectra for the two specimens were obtained at different temperatures ranging between 294 K and 400 K. In this regard, Fig. 4 reports upon the

Table 2
Thermal characteristics of PHB specimens.

Sample	First scan		Second scan	
	Specimen 1	Specimen 2	Specimen 1	Specimen 2
T_{onset} (°C)	167	167	168	161
T_m (°C)	172	176(1)	174	173
ΔH_m (J g^{-1})	–	158(2)	–	–
	69	71	68	66
x_c (%)	47	49	46	45
T_c (°C)	–	–	79	81
ΔH_c (J g^{-1})	–	–	−10	−13

Table 3
Mechanical properties of PHB films.

Sample	Thickness [μm]	E 10^{+3} [MPa]	σ^M [MPa]	ε^M [%]	σ^B [MPa]	ε^B [%]
Speciment 1	54 ± 2	3.78 ± 0,30	29 ± 3	1	29 ± 3	1
Speciment 2	93 ± 4	2.51 ± 0.89	19 ± 1	1	19 ± 1	1
PHB net[a]		1.67 ± 0,50	–	–	21 ± 7	2
PLA[a]		1.15 ± 0,10	–	–	39 ± 2	2

[a] (Reference 22), M (maximum), B (break).

typical results of ESR measurements at four selected temperatures and constant concentration TEMPO ($3.7 \cdot 10^{17}$ spin cm^{-3}).

The temperature dependence of ESR spectral line shapes indicates the changes in the probe rotation rate that is characterized by correlation time (τ_c). In polymer systems, two mechanisms are quite frequently manifested for the spin-probe rotation: one is determined by slow motion with correlation times in the range of 10^{-7}–10^{-9} s rad^{-1}, while the other is characterized by averaged fast motion generating narrowed triplets with τ_c in the range of 10^{-9}–10^{-11} s rad^{-1} [45]. As a rule, in the range of temperatures between T_g and T_M, there are two spin-probe populations with different concentration ratios and diverse impacts on ESR spectral shapes. Each population of TEMPO radicals reflects the proper type of PHB segmental mobility, namely slow or fast dynamics.

In the high temperature range at the rubber-like polymer state (281 K ≈ T_g < T < T_M ≈ 450 K), the slow-motion impact on the spectra is decreased with heating and the probe spectrum in PHB represents the lightly broadened triplet showing the predominance of the fast-motion radical mode due to high segmental mobility. Under these conditions, the anisotropy deficiencies for both the g-factor and the hyperfine splitting constants allow one to regard the polymer medium as the quasi-isotropic matrix. By contrast, when the temperature is decreased to T_g (glassy state), the ESR spectra takes the form corresponding to slow-motion mode of spin rotation (low segmental mobility). In this case, outer components of probe triplet are broadened and shifted away from the central component. Upon further cooling, when the polymer specimen is in glassy-state, the shape of the spectrum is stabilized and the spectrum characteristics weakly depend upon the temperature. The superposition of two rotation modes determines the general shape of spectra and characterizes two different types of polymer micro-environment corresponding to the phase micro-separation in amorphous (polyisoprene) or intercrystalline (PHB) fields of polymers [45,46].

Moreover, based upon Fig. 5 there is evidence that the rotational correlation times (τ_c) are obtained from ESR experiment (points) and fitted to an Arrhenius low (lines) as the function of inverse temperature (K) for two specimens tested. From this Figure, one can observe two different dynamic regimes: one at the high temperature range, where the values of $\ln(\tau_c)$ [s rad^{-1}] are decreased quickly with the inverse temperature and the other at the low-temperature range. The spectra obtained in the vicinity of glass transition temperature of PHB (T_g ≈ 8 ± 1 °C) poorly depends upon temperature and do not provide reliable information on the τ_c values. The latter was indeed not shown in the plot, due to their ambivalence.

The activation energy of the probe rotation (E_r) can be received from the linear fit in accordance with the semilogarithmic function, which was reported below as Eq. (3):

$$\ln(\tau_c) = A_0 + E_r/RT \quad (3)$$

where R is the universal gas constant and A_0 is the pre-exponential factor.

The relations presented in Fig. 5 have the form of the linear function shown in Eq. (3) for the specimen 1 and two intersected lines for the specimen 2. The point of intersection lies in the vicinity of 328 K (54.5 °C) and, hence, there are three values of rotation activation energy determined for two specimens. A special point on the "$\log(\tau_c) - T^{-1}$" relationship for the specimen 2 likely corresponds to the temperature at which the microstructural rearrangement in inter-crystalline fields occurs. Specimen 1 designed via

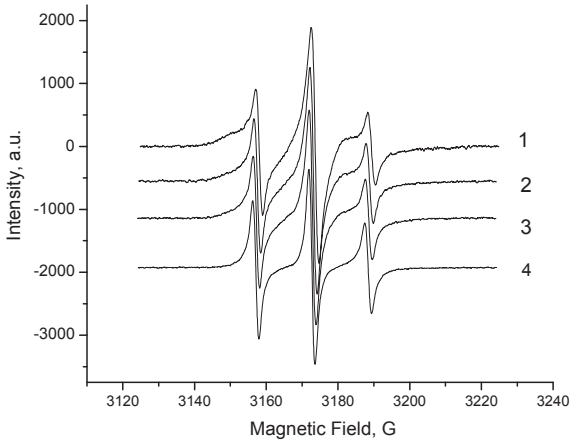

Fig. 4. ESR spectra for probe TEMPO in the PHB specimen 1 at temperatures: 293 K (1), 313 K (2), 333 K (3), 353 K (4). The spectra 2–4 were shifted along the vertical axis.

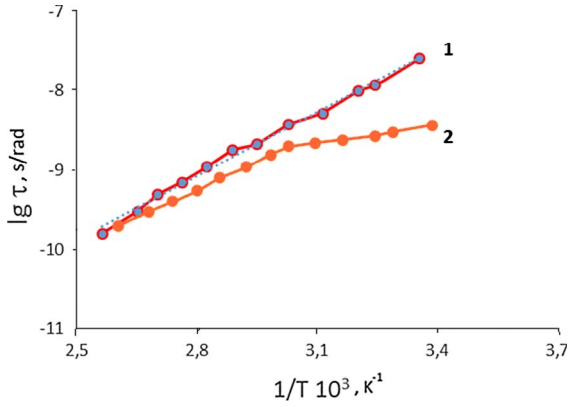

Fig. 5. The rotation time correlation (τ) of the probe (TEMPO) as function of reciprocal absolute temperature in the specimens 1 and 2.

thermo-compressing and characterized by more stable morphology does not manifest any special features in the temperature dependence. Since it is not characterized by a specific delicate structure, it has the highest value of $E_\tau = 51 \pm 3\ kJ\ mol^{-1}$. At the same, time the specimen 2 with the globular morphology has $E_\tau = 40 \pm 3\ kJ\ mol^{-1}$ in the high-temperature range, 400–328 K (127–55 °C), and the further sharp drop to the value of $15 \pm 2\ kJ\ mol^{-1}$.

Analogous temperature transitions of ESR probe dynamics in polymer systems have been observed in a number of recently published papers [47]. In this context, it is worth to emphasize that a weak endothermic peak has been recently found at ~332 K on DSC thermo-grams of the PHB-drug system [48]. Besides, an analogous, more pronounced peak has been registered for polylactide with similar structural characteristics [49]. DSC endothermic peaks for both polymers are tentatively related with enthalpy relaxation or structural relaxation [49,50]. As a matter of fact, there is an extremely weak analogy between dynamic regimes and thermal transitions in PHB. Therefore, the nature of such dynamical transitions, described in our case and in the literature, still remains unclear until the end.

3.6. Gas transport through the PHB film

Under constant upstream pressure (p_f) and temperature conditions, the amount of gaseous penetrant (Q_t) transferring through the PHB film per unit area is given by Eq. 4 formulated by Crank [51].

Assuming that gas equilibrium at the upstream interface of polymer is instantly established and that the gas concentration in PHB is low enough, it can be written a simple expression for a gas Henry's law (see Eq. 5).

At large times, the Eq. 5 can be written as showed in Eq. 6. For greater understanding, Eqs. 4, 5 and 6 were shown in Table 4.

For gaseous penetrants, namely CO_2, O_2, N_2, and C_2H_4, the gas pressure rise in the low-pressure chamber was recalculated to receive the corresponding permeability data as gas transmission rates (GTR), which are presented in Fig. 6.

Additionally, the transport results were reported in Table 5, for specimen 1. GTR values of specimen 2 were very high and, due to the high polymer porosity, it could not be analyzed as barrier material. The gas permeabilities data were computed by fitting the linear Eq. 6 to experimental data, while the diffusion coefficients were evaluated by Eq. (7):

$$D = L^2/t_D \tag{7}$$

where t_D is the intercept of the line in coordinates Q − t from Eq. (6) on the t-axes [51,52].

The given group of gaseous penetrants has been chosen for the investigation because their transport characteristics (permeability, diffusivity, and sorption) determine predominantly the quality food storage. The above illustrations follow that PHB presents good barrier features due to low GTR values not only for oxygen but for CO_2 as well.

The high crystallinity of the biopolymer (~50%) imparts the macromolecular rigidity and the decrease of free volume ratio,

Table 4
Equations used for the calculation of gas transport through the PHB films [51,62].

$\frac{Q_t}{L \times c_f} = \frac{D \times t}{L^2} - \frac{1}{6} - \frac{1}{\pi^2} \times \sum_{n=1}^{\infty} \left[\frac{(-1)^2}{n^2} \right] \left(-\frac{D \times n^2 \times \pi^2 \times t}{L^2} \right)$	(4)
$c_f = S \times p_f$	(5)
$\frac{L \times Q_t}{p_f} = D \times S \times \left(t - \frac{L^2}{6 \times D} \right) = P \times \left(t - \frac{L^2}{6 \times D} \right)$	(6)

L is the membrane thickness; c_f and p_f are the upstream gas concentration and pressure, respectively; D is the diffusion coefficient of the gaseous penetrant; t is the experimental time; S is the Henry's coefficient expressing the gas solubility; P is the gas permeability defined as the product of diffusivity (D) and solubility (S).

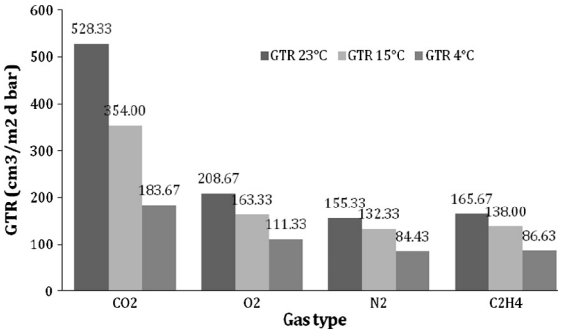

Fig. 6. Comparison of gas permeabilities (GTR) through the PHB film, at different temperatures.

hindering the gas fluxes through the films. With that, at selected temperatures the ratio of CO_2/O_2 permeabilities (i.e. perm-selectivity) was more than two (see Table 5) that is important for food packaging systems. The basic concept of free volume being responsible for gas diffusion is well suited for describing transport processes in barrier polymer materials both above and below glass-transition temperatures [53–58]. In the fundamental work, Cohen and Turnbull separated the total free volume into the portions of infinitely small constituent volumes with different sizes and derived their distribution to obtain the final expression for gas diffusivity, as showed in Eq. (8) [59–60]:

$$D = D_0^{(-\alpha \times v^*/v_f)} \tag{8}$$

where D_0 could be taken for the Chapmen-Enskog self-diffusion coefficient; α is the correction factor; v^* is the adjustable constant related to the elementary critical volume into which a gas molecule is enabled to pass and v_f is the mean free volume in the amorphous fraction of PHB [60,61].

Assuming that $\alpha \times v^* = k \times V_{cc}$ the Eq. (8) can be easily converted to the Eq. (9):

$$D = D_0^{(-k \times V_{cc}/v_f)} \tag{9}$$

in which k_f is a novel correlation factor and V_{cc} is the critical volume of the gaseous penetrant. Taking this assumption, it is expected that the critical volume of gas is proportional to the elementary minimum free volume to be capable of accommodating a gas molecule.

For O_2, CO_2, and N_2, the semi-logarithmic dependence of diffusivity on the critical volume is shown in Fig. 7, which agrees reasonably with Eq. (9).

The molecular diameter and critical volume of O_2 are less than the corresponding characteristics of CO_2. Therefore, in accordance with both the Eyring-Barrer activation theory and the free volume model of gas transport, oxygen diffusivity is essentially higher than that of composite carbon dioxide molecules [62,63].

The opposite situation was observed for the gas solubility in PHB. Here it is evident the good affinity of CO_2 to the ester groups of PHB: therefore, its solubility exceeds by the three orders of magnitude the O_2 solubility. Taking into account that gas permeability is the product of diffusivity and solubility, its higher values for CO_2 ascertaining at all temperatures testify the high contribution of thermodynamic solubility into total transport process. Higher partial permeability of CO_2 compared to the other gases such as N_2,

Table 5
Gas transports characteristics for PHB at different temperatures, for specimen 1.

Temperature (K)	GTR10^{-2} ($cm^3\ cm^{-2}\ d^{-1}\ bar^{-1}$)	$t_L\ 10^{-3}$ (s)	S ($cm^3\ cm^{-2}\ bar^{-1}$)	D 10^{10} ($cm^2\ s^{-1}$)
CO_2				
277	1.84 ± 0.01	9.92 ± 0.10	2.30 ± 0.03	4.8 ± 0.2
288	3.54 ± 0.03	3.84 ± 0.57	1.90 ± 0.10	12.0 ± 0.9
296	5.28 ± 0.01	5.08 ± 0.45	3.50 ± 0.04	9.6 ± 0.8
O_2				
277	1.10 ± 0.01	0.674 ± 0.41	9.710^{-4} ± 0.6210^{-4}	72.0 ± 4.2
288	1.63 ± 0.01	–	–	–
296	2.09 ± 0.01	–	–	–
N_2				
277	0.84 ± 0.05	6.35 ± 0.06	0.69 ± 0.02	7.70 ± 0.08
288	1.32 ± 0.01	–	–	–
296	1.55 ± 0.01	–	–	–
C_2H_4				
277	0.87 ± 0.02	–	–	–
288	1.38 ± 0.01	–	–	–
296	1.66 ± 0.01	–	–	–

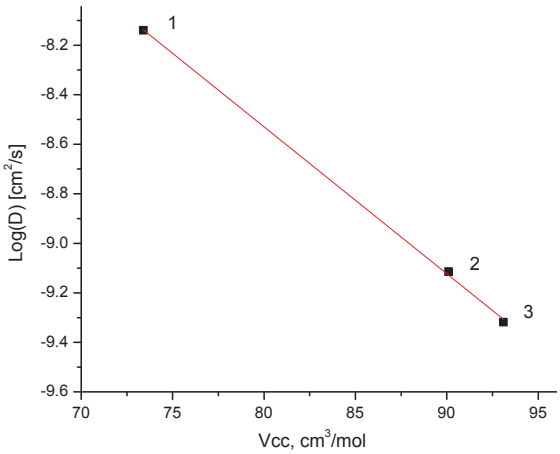

Fig. 7. Semi-logarithmic dependence of gas diffusivities of corresponding critical gas volume. 1 – O_2, 2 – N_2, 3 – CO_2.

C_2H_4 and O_2 creates favourable prerequisites for the PHB application as a selective barrier material.

As it can be observed from the above data, the greatest effect of temperature on permeability increment was observed for carbon dioxide. To compare all temperature dependences of gas permeabilities the Arrhenius-Barrer approach was used to allow the calculation of their activation energies (E_P), as well as in the activation energies of gas diffusion (E_D). Additionally, the gas solubility dependences upon the temperature were recorded in terms of Van't Hoff relationship, so enabling calculation of the partial molar enthalpies of the process (H_S) [64].

Following the classical approaches of temperature-activated diffusion of Eyring-Barrer and free volume theory of Yasuda, the GTR increment with temperature, as documented in literature, is mostly related to: (i) the motion of the polymer segments; (ii) the size of gaseous penetrants; and (iii) the increased energy level of permeating molecules and polymeric chain packing [62,64–67].

The temperature dependence of permeability for the given gases is represented by an Arrhenius relationship (Eq. (10)):

$$P = P_0^{(-E_P/R\times T)} \tag{10}$$

where P_0 is a pre-exponential factor; E_P is the apparent activation energy for permeation; T is the absolute temperature (K) and R is the universal gas constant.

Permeability was calculated at different temperatures, namely at 4, 15 and 23 °C. The values of E_P for all gases have been determined from the slope of the plot in semilogarithmic coordinates, log P versus 1/T, as showed in Fig. 8. For comparison all data were presented in Table 6.

In the same way, the temperature dependence of the gas diffusion coefficients can be represented and calculated by an Arrhenius relationship (Eq. (11)):

$$D = D_0^{(-E_D/R\times T)} \tag{11}$$

where D_0 is a pre-exponential factor, and E_D is the activation energy for diffusion.

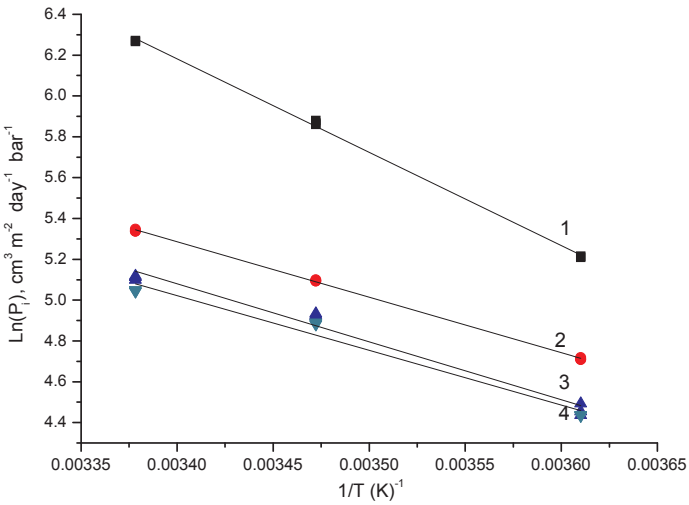

Fig. 8. Temperature dependence of gas permeability in the coordinates of Arrhenius Equation: CO_2 (1), O_2 (2), C_2H_4 (3), and N_2 (4).

Table 6
The energy activations of permeability (GTR) for gaseous penetrants (E_P), the corresponding characteristic of diffusivity (E_D) for CO_2 and the apparent heat of equilibrium sorption (H_S) for CO_2, with R^2-factors between parentheses.

Penetrant	E_P [kcal mol^{-1}]	E_D [kcal mol^{-1}]	H_S [kcal mol^{-1}]
CO_2	9.1 ± 0.1 (0.999)	3.1 ± 0.8 (0.571)	6.4 ± 0.7 (0.910)
O_2	5.4 ± 0.1 (0.999)	–	–
N_2	5.3 ± 0.3 (0.972)	–	–
C_2H_4	5.7 ± 0.3 (0.975)	–	–

The temperature dependence of gas solubility in polymers has been described using a thermodynamic van't Hoff expression that was reported in Eq. (12):

$$S = S_0^{(-H_S/R\times T)} \tag{12}$$

where S_0 is a pre-exponential factor, and H_S is the apparent heat of equilibrium sorption [64]. The corresponding results of calculation E_D and H_S for CO_2 were shown in the same Table 6.

The given group of the gaseous penetrants has been chosen for this investigation because of theirs transport characteristics (permeability, diffusivity, and equilibrium sorption) determine predominantly the food quality during storage and the shelf-life. The data are being presented in Fig. 8 and Table 6 shows that PHB exhibits the good barrier features owing to the low GTR values of oxygen, carbon dioxide and the other gases investigated.

Additional comparison of the gas permeabilities at selected temperatures was carried out by the calculation of the "perm-selectivity" values that are the pairwise relationships of the gas GTR values taken from Table 6. The results of perm-selectivity calculations can be seen in Table 7. These data could be helpful for the evaluation of the polymer barrier characteristics. When the value of the first gas is experimentally determined, the value for the second gas can be calculated using the corresponding perm-selectivity meaning.

As can be observed in Table 7, the perm-selectivity values for the pairs of gaseous penetrants containing carbon dioxide (CO_2/O_2, CO_2/N_2, and CO_2/C_2H_4) depend upon the temperature positively, whereas the same barrier characteristics for the pairs of O_2/N_2 and O_2/C_2H_4 are almost equal to each other and do not depend on the temperature as well. The latter result is not obvious, but it has certain analogies under an oxygen transport consideration. As it has been show by Gordon [68], at isothermal conditions the perm-selectivity of poor condensable gases, such as O_2, N_2, and CO_2, are constant and not affected by a chemical structure of polymers. Here, in this publication, the author reported that the perm-selectivity values of those gases decreased with the temperature increase. In case of PHB, the detected positive impact of the temperature on the CO_2 perm-selectivity is in some contradiction with Gordon's results, though the general gas perm-selectivity trend is in consistent with the diffusivity and permeability dependences on the temperature.

4. Conclusion

Innovative technology transfer from the traditional packaging based on synthetic polymers to the biodegradable barrier materials is directly associated with intensive scientific and applied researches. The proposed complex examination can be applied not only for the strongly determined family of polymers, polyhydroxyalkanoates, but also for other biodegradable polymeric materials such as polylactides, polysaccharides, proteins and others. The further development of this type of work will be aimed at development of biocomposites with encapsulated nanoparticles (TiO_2, Fe_3O_4) [69]. Preparation and characterization of biodegradable nanocomposites should lead to the design of "smart" packaging, i.e. stimuli-responsive barrier materials with an immediate reaction on environmental changes such as humidity, external magnetic field, pH, mechanical impact and others.

The physicochemical characteristics, segmental dynamics, and gas transport properties (i.e., permeability, diffusivity, and solubility) of PHB films were coherently investigated by the complex of relevant methods. Additionally, the SEM technique shows that the surfaces of PHB films acquire morphologies with the coalescing spherical globules incorporated into the polymer matrix. For the solution-cast films, there were a large number of pores formed as a result of loosely connected globules. In contrast to cast specimens of PHB, the surfaces of thermo-compressed films have a uniform globular pattern with single or coalescing spherical particles which are tightly embedded into the matrix without visible defects or pores.

In the selected range of temperatures (277–296 K), the ranking of the gas permeabilities (P_i) for the thermo-compressed films has the following sequence: $P(CO_2) > P(O_2) > P(N_2) \approx P(C_2H_4)$. For this group of gases, there is no direct correlation between the

Table 7
Calculated gas perm-selectivity data for the PHB films.

Temperature (K)	CO_2/O_2	CO_2/N_2	CO_2/C_2H_4	O_2/N_2	O_2/C_2H_4
277	1.7	2.2	2.1	1.3	1.3
288	2.2	2.7	2.7	1.2	1.2
296	2.5	3.4	3.2	1.3	1.3

permeability and the gas molecule size. It is quite understandable, because in the framework of the solubility-diffusion model, the coefficient of permeability as a molecular characteristic includes diffusivity and solubility coefficients simultaneously. Each of them has the proper dependence on molecular geometry of gaseous penetrants. Hence, the superposition of two inconsistent trends may give a sophisticated form of permeability function. In this work, it was shown the apparent diffusion coefficients dependence on the critical volumes of atmospheric gases (CO_2, O_2 and N_2) as the semi-logarithmic function. This relation manifests that the free volume model could be applied for description of gas transport in high crystalline polymers such as PHB and PLA.

The activation energies of gas permeabilities, diffusivities, and spin probe rotation, as well as the apparent heat of equilibrium sorption gain the opportunity to predict the values of PHB transport characteristics in the practically important interval of temperatures at which foodstuffs are stored. The series of additional examinations including calorimetric, mechanical and thermal characteristics are devoted to the database creation with the objective to use the biodegradable polyester as barrier materials in packaging and medicine applications.

References

[1] Y. Masse, K. Liesl, Permeability Properties of Plastic and Elastomers: A Guide to Packaging and Barrier Materials, Plastic Design Library, William Andrew Publishing, Norwich, New York, USA, 2003, pp. 615–616 (ISBN 1-884207-97-9).
[2] J. Peyroux, M. Dubois, E. Tomasella, L. Frézet, A.P. Kharitonov, D. Flahaut, Enhancement of surface properties on Low Density Polyethylene packaging films using various fluorination routes, Eur. Polym. J. 66 (2015) 18–32.
[3] Y. Yampolskii, I. Pinnau, B. Freeman (Eds.), Materials Science of Membranes for Gas and Vapor Separation, John Wiley & Sons Ltd, Chichester, England, 2006.
[4] K. Marsh, E.B. Bugusu, Food packaging: roles, materials, and environmental, J. Food Sci. 72 (3) (2007) R39–R55.
[5] V. Siracusa, P. Rocculi, S. Romani, M. Dalla Rosa, Biodegradable polymers for food packaging: a review, Trends Food Sci. Technol. 19 (2008) 634–643.
[6] R.N. Tharanathan, Review e biodegradable films and composite coatings: past, present and future, Trends Food Sci. Technol. 14 (2003) 71–78.
[7] M. Bishai, S. De, B. Adhikari, R. Banerjee, A comprehensive study on enhanced characteristics of modified polylactic acid based versatile biopolymer, Euro. Polym. J. 54 (2014) 52–61.
[8] J.H. Song, R.J. Murphy, R. Narayan, G.B.H. Davies, Biodegradable and compostable alternatives, Phil. Trans. R. Soc. B 364 (2009) 2127–2139.
[9] X. Wen, X. Lu, Microbial degradation of poly(3-hydroxybutyrate-co-4-hydroxybutyrate) in soil, J. Polym. Environ. 20 (2) (2012) 381–387.
[10] D.Z. Bucci, L.B.B. Tavares, I. Sell, PHB packaging for the storage of food products, Poly. Test. 24 (5) (2005) 564–571.
[11] K.M. Zia, A. Noreena, M. Zuber, S. Tabasum, M. Mujahid, Recent developments and future prospects on bio-based polyesters derived from renewable resources: a review, Int. J. Biol. Macromol. 82 (2016) 1028–1040.
[12] A.L. Iordanskii, G.A. Bonartseva, Y.N. Pankova, S.Z. Rogovina, K.Z. Gumargalieva, G.E. Zaikov, A.A. Berlin, Current status and biomedical application spectrum of poly(3-hydroxybutyrate as a bacterial biodegradable polymer, in: D. Balkose, D. Horak, L. Soltes (Eds.), Current State-of-the-Art on Novel Materials, vol. 1, Apple Academic Press, New York, USA, 2013, pp. 253–296 (Chapter 12).
[13] S. Modi, K. Koelling, Y. Vodovotz, Assessment of PHB with varying hydroxyvalerate content for potential packaging applications, Euro. Polym. J. 47 (2011) 179–186.
[14] A. Bergstrand, S. Uppström, A. Larsson, Permeability of porous poly(3-hydroxybutyrate) barriers of single and bilayer type for implant applications, Int. J. Polym. Sci. (2014) Article ID 958975.
[15] J.S. Yoon, H.W. Jung, M.N. Kim, E.S. Park, Diffusion coefficient and equilibrium solubility of water molecules in biodegradable polymers, J. Appl. Polym. Sci. 77 (2000) 1716–1722.
[16] F.C. Godoi, N.R. Pereira, S.C.S. Rocha, Analysis of the drying process of a biopolymer (poly-hydroxybutyrate) in rotating-pulsed fluidized bed, Chem. Eng. Proc. 50 (2011) 623–629.
[17] P.P. Kamaev, A.L. Iordanskii, I.I. Aliev, A.W. Wasserman, U. Hänggi, Transport water and molecular mobility in novel barrier membranes with different morphology features, Desalination 126 (1999) 153–157.
[18] N. Follain, C. Chappey, E. Dargent, F. Chivrac, R. Crétois, S. Marais, Structure and Barrier properties of biodegradable PHA films, J. Phys. Chem. C 118 (12) (2014) 6165–6177.
[19] S. Domenek, M. Pronnier, V. Ducruet, Barrier properties of biodegradable polyesters to aroma compounds, Res. Gate Dateset (2015), <http://www.researchgate.net/publication/273126336>.
[20] Y.M. Corre, S. Bruzaud, J.L. Audic, Y. Grohens, Morphology and functional properties of commercial polyhydroxyalkanoates: a comprehensive and comparative study, Polym. Test. 31 (2) (2012) 226–235.
[21] J. Vandewijngaarden, M. Murariu, P. Dubois, R. Carleer, J. Yperman, P. Adriaensens, R. Peeters, M. Buntinx, Gas permeability properties of poly(3-hydroxybutyrate-co-3-hydroxyhexanoate), J. Polym. Environ. Open Access. (2014). http://dx.doi.org/10.1007/s10924-014-0688-1.
[22] M.P. Arrieta, E. Fortunati, F. Dominici, E. Rayón, J. López, J.M. Kenny, PLA-PHB/cellulose based films: mechanical, barrier and disintegration properties, Polym. Degr. Stab. 107 (2014) 139–149.
[23] M.P. Arrieta, J. López, A. Hernández, E. Rayón, Ternary PLA-PHB-Limonene blends intended for biodegradable food packaging applications, Euro. Polym. J. 50 (2014) 255–270.
[24] I. Armentano, E. Fortunati, N. Burgos, F. Dominici, Francesca Luzi, Stefano Fiori, A. Jiménez, K. Yoon, J. Ahn, S. Kang, J.M. Kenny, Bio-based PLA-PHB plasticized blend films: Processing and structural characterization, LWT - Food Sci. Technol. 64 (2) (2015) 980–988.
[25] S. Mattioli, M. Peltzer, E. Fortunati, I. Armentano, A. Jiménez, J.M. Kenny, Structure, gas-barrier properties and overall migration of poly(lactic acid) films coated with hydrogenated amorphous carbon layers, Carbon 63 (2013) 274–282.
[26] M.A. Ortenzi, L. Basilissi, H. Farina, G. Di Silvestro, L. Piergiovanni, E. Mascheroni, Evaluation of crystallinity and gas barrier properties of films obtained from PLA nanocomposites synthesized via “in situ” polymerization of l-lactide with silane-modified nanosilica and montmorillonite, Euro. Polym. J. 66 (2015) 478–491.
[27] V. Siracusa, C. Ingrao, The use of polylactic acid in food packaging, Reference Module in Food Sciences, Elsevier, 2016http://dx.doi.org/10.1016/B978-0-08-100596-5.03208-X pp. 1.
[28] S.G. Karpova, A.L. Iordanskii, M.V. Motyakin, A.A. Ol’khov, S.Z. Rogovina, A.A. Berlin, Structural–dynamic characteristics of matrices based on ultrathin poly(3-hydroxybutyrate) fibers prepared via electrospinning, Polym. Sci. Ser. A 57 (2) (2015) 131–138.
[29] S. Galus, A. Lenart, Development and characterization of composite edible films based on sodium alginate and pectin, J. Food Eng. 115 (2013) 459–465.
[30] K. Syahidad, S. Rosnah, M.A. Noranizan, O. Zaulia, A. Anvarjo, Quality change of fresh cut cantaloupe (Cucumis melo L.) in different types of polypropylene packaging, Int. Res. J. 22 (2) (2015) 753–760.
[31] P.J. Barham, A. Keller, E.L. Otun, P.A. Holmes, Crystallization and morphology of a bacterial thermoplastic: poly-3-hydroxybutyrate, J. Mater. Sci. 19 (9) (1984) 2781–2794.
[32] S.S. Eaton, G.R. Eaton, L.J. Berliner (Eds.), Biomedical EPR - Part B: Methodology, instrumentation, and dynamics, Biological Magnetic Resonance, vol. 24, Springer-Verlag, 2005ISBN: 0-306-48532-X.
[33] D.E. Budil, S. Lee, S. Saxena, J.H. Freed, Nonlinear-least-squares analysis of slow-motion EPR spectra in one and two dimensions using a modified levenberg–marquardt algorithm, J. Magn. Res. Ser. A 120 (1996) 155–189.
[34] V.P. Timofeev, V.I. Tsetlin, Analysis of mobility of protein side-chains by spin label technique, Biophys. Struct. Mech. 10 (1983) 93–108.

[35] V. Siracusa, Food packaging permeability behaviour: a report, Int. J. Polym. Sci. 1 (2012) 1–11.
[36] S. Mrkic, K. Galic, M. Ivankovic, S. Hamin, N. Cikovic, Gas transport and thermal characterization of mono-and di-polyethylene films used for food packaging, J. Appl. Polym. Sci. 99 (2006) 1590–1598.
[37] S. Pao, G.E. Brown, K.R. Schneider, Challenge studies with selected pathogenic bacteria on freshly peeled hamlin orange, J. Food Sci. 63 (1998) 359–362.
[38] I. Marklinder, M.K. Eriksson, Best-before date – food storage temperatures recorded by Swedish studentsBrit, Food J. 117 (2015) 1764–1776.
[39] D. Seebach, A. Brunner, B.M. Bachmann, T. Hoffmann, F.N.M. Kühnle, U.D. Lengweiler, Biopolymers and Oligomers of (R)-3-Hydroxyalkanoic Acids, Contribution of Synthetic Organic Chemists, Ernst Schering Foundation, Berlin, 1995.
[40] G. Espín, M. Castañeda, J. Guzmán, S. Moreno, G. Espin, The GacS sensor kinase regulates alginates and poly-β-hydroxybutyrate production in azotobacter vinelandii, J. Bacteriol. 182 (9) (2000) 2624–2628.
[41] M.C. Righettia, M.L. Di Lorenzo, Melting temperature evolution of non-reorganized crystals. Poly(3-hydroxybutyrate), Thermochim. Acta 512 (2011) 59–66.
[42] R. Pearce, R.H. Marchessault, Multiple melting in blends of isotactic and atactic poly(β hydroxybutyrate), Polymer 35 (1994) 3990–3997.
[43] J. Zhang, H. Sato, T. Furukawa, H. Tsuji, I. Noda, Y. Ozaki, Crystallization behaviors of poly(3-hyroxybutyrate) and poly(l-lactic acid) in their immiscible and miscible blends, J. Phys. Chem. B 110 (2006) 24463–24471.
[44] L.M.W.K. Gunaratne, R.A. Shanks, Thermal memory of PHB using temperature modulated differential scanning calorimetry, J. Polym. Sci. Part B: Polym. Phys. 44 (1) (2006) 70–78.
[45] J. John, D. Klepac, M. Didović, C.J. Sandesh, Y. Liu, K.V.S.N. Raju, A. Pius, S. Valić, S. Thomas, Main chain and segmental dynamics of semi interpenetrating polymer networks based on polyisoprene and poly(methyl methacrylate), Polymer 51 (2010) 2390–2402.
[46] J. John, D. Klepac, M.P. Didović, K.V.S.N. Raju, A. Pius, M. Andreis, S. Valić, S. Thomas, Relaxations and chain dynamics of sequential full interpenetrating polymer networks based on natural rubber and poly(methyl methacrylate), Polym. Int. 63 (8) (2013) 1427–1438.
[47] P.P. Kamaev, I.I. Aliev, A.L. Iordanskii, A.M. Wasserman, Molecular dynamics of the spin probes in dry and wet poly(3-hydroxybutyrate) films with different morphology, Polymer 42 (2001) 515–520.
[48] A.L. Iordanskii, A.A. Olkhov, S.G. Karpova, E.L. Kucherenko, R. Yu. Kosenko, S.Z. Rogovina, A.E. Chalykh, A.A. Berlin, Effect of structure and morphology of ultrathin PHB fibers on diffusion and transport of drug, Polym. Sci. Rus. A (2016) (unpublished).
[49] V.M. Correlo, L.F. Boesel, M. Bhattacharya, J.F. Mano, N.M. Neves, R.L. Reis, Properties of melt processed chitosan and aliphatic polyester blends, Mater. Sci. Eng. A403 (2005) 57–68.
[50] S.C. Lee, J.I. Han, Y.G. Jeong, M. Kwon, Strain-induced enthalpy relaxation in poly(lactic acid), Macromolecules 43 (2010) 25–28.
[51] J. Crank, The Mathematics of Diffusion, third ed., Clarendon Press, Oxford, UK, 1992.
[52] P. Taveira, A. Mendes, C. Costa, On the determination of diffusivity and sorption coefficients using different time-lag models, J. Membr. Sci. 221 (1–2) (2003) 123–133.
[53] B.D. Freeman, I. Pinnau, Polymeric materials for gas separations, in: B.D. Freeman, I. Pinnau (Eds.), Polymer Membranes for Gas and Vapor Separation, ACS Symposium Series, American Chemical Society, Washington DC, 1999, pp. 1–27 (Chapter 1).
[54] L.I. Costa, G. Storti, Self-diffusion of small molecules into rubbery polymers: a lattice free-volume theory, J. Polym. Sci. Part B Polym. Phys. 48 (5) (2010) 529–540.
[55] M.P. Tonge, R.G. Gilbert, Testing free volume theory for penetrant diffusion in rubbery polymers, Polymer 42 (4) (2001) 1393–1405.
[56] P.N. Patil, D. Roilo, R.S. Brusa, A. Miotello, S. Aghion, R. Ferragut, R. Checchetto, Free volumes and gas transport in polymers: amine-modified epoxy resins as a case study, Phys. Chem. Chem. Phys. 18 (5) (2016) 3817–3824.
[57] M.G. Baschetti, F. Doghieri, B. Freeman, G.C. Sarti, Transient and steady state effective diffusivity in high free volume glassy polymers, J. Membr. Sci. 344 (1–2) (2009) 144–154.
[58] L.M. Robeson, Z.P. Smith, B.D. Freeman, D.R. Paul, Contributions of diffusion and solubility selectivity to the upper bound analysis for glassy gas separation membranes, J. Membr. Sci. 453 (2014) 71–83.
[59] M.H. Cohen, D. Turnbull, Molecular transport in liquids and glasses, J. Chem. Phys. 31 (1959) 1164–1169.
[60] R. Laghaei, A.E. Nasrabad, B.C. Eu, Generic van der Waals equation of state, modified free volume theory of diffusion, and viscosity of simple liquids, J. Phys. Chem. B 109 (2005) 5873–5883.
[61] R.A. Reis, R. Nobrega, F.W. Tavares, J.V. Oliveira, Mutual diffusion coefficient models for polymer-solvent systems based on the chapman-enskog theory, Braz. J. Chem. Eng. 21 (04) (2004) 611–619.
[62] R.M. Barrer, G. Skirrow, Transport and equilibrium phenomena in gas–elastomer systems. I. Kinetic phenomena, J. Polym. Sci. Part A Polym. Chem. 3 (4) (1948) 465–608.
[63] J. Crank, G.S. Park, Diffusion in Polymers, Academic Press, London and New York, 1968p. 452.
[64] S. Matteucci, Y. Yampolskii, B.D. Freeman, I. Pinnau, Transport of gases and vapors in glassy and rubbery polymers, in: Y. Yampolskii, I. Pinnau, B.D. Freeman (Eds.), Materials Science of Membranes for Gas and Vapor Separation, John Wiley & Sons Ltd., Chichester, 2006, pp. 1–48.
[65] R.M. Barrer, Diffusivities in glassy polymers for the dual mode sorption model, J. Membr. Sci. 18 (1984) 25–35.
[66] S.S. Jordan, W.J. Koros, A free volume distribution model of gas sorption and dilation in glassy polymers, Macromolecules 28 (1995) 2228–2235.
[67] V. Siracusa, N. Lotti, A. Munari, M. Dalla Rosa, Poly(butylene succinate) and poly(butylene succinate-co-adipate) for food packaging applications: gas barrier properties after stressed treatments, Polym. Degr. Stab. 119 (2015) 35–45.
[68] G.L. Robertson, Food Packaging: Principles and Practice, second ed., Marcel Dekker, New York, 2006Chapter 4, pp. 63–64.
[69] A.L. Iordanskii, A.V. Bychkova, K.Z. Gumargalieva, A.A. Berlin, Magnetoanisotropic biodegradable nanocomposites for controlled drug release, in: W. Andrew (Ed.), Applications of Nanobiomaterials (Multi-Volume SET I-XI), NanoBioMaterials in Drug Delivery, vol. IX, Elsevier, Amsterdam-Boston, 2016, pp. 171–196 (Chapter 6).